The accretion-ejection connexion in T Tauri stars: jet models vs. observations

S. Cabrit

LERMA, Observatoire de Paris, UPMC, CNRS, 61 Av. de l'Observatoire, 75014 Paris, France
email: Sylvie.Cabrit@obspm.fr

Abstract. Key observational constraints for jet models in T Tauri stars are outlined, including the jet collimation scale, kinematic structure, and ejection/accretion ratio. It is shown that MHD self-collimation is most likely required. The four possible MHD ejection sites (stellar surface, inner disk edge, extended disk region, magnetosphere-disk reconnexion line) are then critically examined against observational constraints, and open issues are discussed.

Keywords. Hydrodynamics, stars: pre–main-sequence, stars: winds, outflows, ISM: jets and outflows.

1. Introduction: key properties of spatially resolved T Tauri jets

Modelling of Helium and Hydrogen line profiles in classical T Tauri stars (CTTS) suggests the presence of inner winds from the star or the inner disk edge (see reviews by S. Edwards and by S. Alencar, this volume). The contribution of these winds to the large scale jets observed in forbidden lines and to the angular momentum regulation of CTTS is still unclear, however. In this review, I will approach the problem from the other end and use asymptotic properties beyond 15 AU derived from spatially resolved forbidden line observations (see T. Ray, this volume) to test proposed models for T Tauri jets. These properties include:

- *1. Jet collimation:* the opening angle drops from $20° - 30°$ initially to a few degrees beyond 50 AU of the source, where the apparent jet HWHM radius reaches $\simeq$ 10–20 AU (Hartigan *et al.* 2004; Ray *et al.* 1996; Dougados *et al.* 2000).
- *2. Jet terminal speeds*: the high-velocity component (HVC) typically reaches $\simeq$ 200 to 350 km s^{-1} after deprojection, i.e.,g $1 - 2$ times the stellar keplerian speed, within 15 AU of the source (Bacciotti *et al.* 2000; Woitas *et al.* 2002).
- *3. Transverse velocity decrease:* several jets exhibit an intermediate velocity component (IVC) at 100–10 km s^{-1}, arising from a slower sheath at $\simeq$ 15–30 AU of the jet axis (Lavalley-Fouquet *et al.* 2000; Bacciotti *et al.* 2000; Coffey *et al.* 2004; Coffey *et al.* 2007).
- *4. Jet rotation:* the specific angular momentum at the jet outer edge could be up to $100 - 300$ AU km s^{-1}; it would be lower if other effects than rotation are present (Bacciotti *et al.* 2002; Coffey *et al.* 2004; Cabrit *et al.* 2006; Cerqueira *et al.* 2006).
- *5. Jet ejection/accretion ratio:* current best estimates lead to a *two-sided* value of $\simeq$ 0.1–0.2 (see below).

Recent advances on jet heating and jet mass fluxes are reviewed in § 2, while § 3 presents several arguments in favor of MHD self-collimation of CTTS jets. § 3–6 then confront the possible jet origins (star, inner disk edge, extended disk region, magnetosphere-disk reconnexion site) with the above observational constraints. Concluding remarks are presented in § 8.
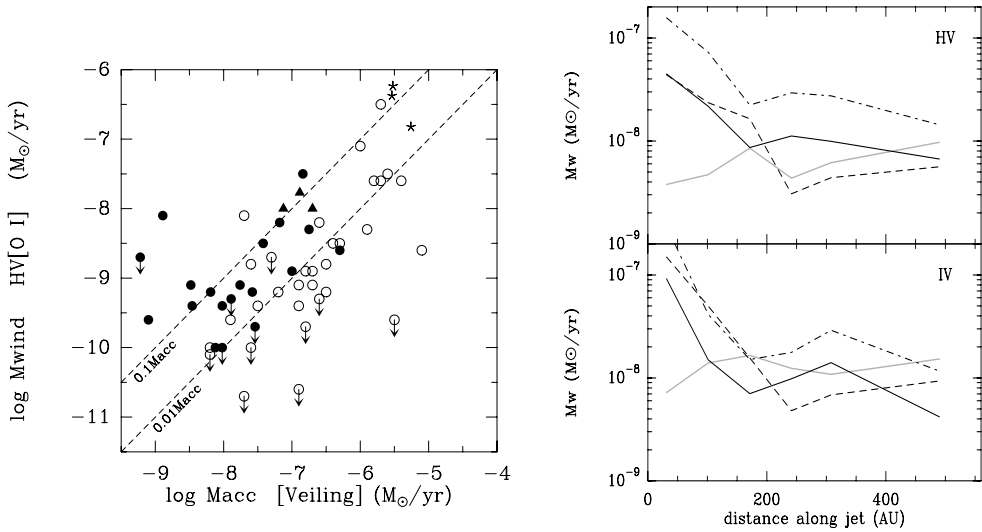
Figure 1. *Left:* Correlation of ejection rate in the blueshifted jet to accretion rate from veiling in CTTS. Open circles are data from HEG95. Filled circles use revised $\dot{M}_{acc}$ from Muzerolle *et al.* 1998. The 3 microjets with updated $\dot{M}_j$ from spectroimaging are denoted as filled triangles, and the 3 Class I jets as asterisks. The mean one-sided $\dot{M}_j/\dot{M}_{acc}$ is 0.05–0.1. From Cabrit *et al.* in prep. *Right:* Mass-loss rates in the HVC and IVC of DG Tau obtained with the 4 methods described in the text (A.1: dash-dot, A.2: solid, B.1: grey, B.2: dashed). From Cabrit (2002).

2. Jet mass-flux and ejection/accretion ratio

The good correlation of [OI] jet brightness with mid-infrared excess from the inner disk and with optical excess from the hot accretion layer reveals that jets are ultimately powered by accretion (Cabrit *et al.* 1990; Hartigan *et al.* 1995, hereafter HEG95). The ejection/accretion ratio is then a key parameter to constrain the jet acceleration mechanism and launch site. HEG95 inferred a mean *one-sided* ratio $\dot{M}_j/\dot{M}_{acc} \simeq 0.01$ (see open circles in left panel of Figure 1), but updated accretion rates using revised bolometric corrections and A_V are on average 10 times smaller (Muzerolle *et al.* 1998). This would suggest a 10 times higher ratio, provided $\dot{M}_j$ does not suffer from a similar bias.

Significant progress on CTTS jet mass-flux estimates have been made recently thanks to sub-arcsecond spectroimaging: as shown in Fig. 2, spatially-resolved line ratios in microjets demonstrate that heating is dominated by shocks beyond 30 AU, and yield estimates of shock parameters and postshock density as a function of distance and velocity. The mass-flux can then be cross-checked using 4 different methods: one may either use the jet mean density and radius (option A), or the [OI] line luminosity (option B); and in each case one may assume either (1) a uniform emissivity within the beam, or (2) a single shock wave (see Cabrit 2002 for a detailed review).

A comparison of the 4 methods in the DG Tau jet is presented in the right panel of Fig. 1. They agree to within a factor 3 beyond 150 AU, but greatly diverge closer in. This could be due to the steeper gradients in physical conditions close to the star, and to the larger uncertainties in A_V and jet radius there. "Asymptotic" mass-loss rate values beyond 150 AU ($t_{dyn} \simeq 3$ yrs) are therefore more reliable.

Comparing with earlier mass-loss rates obtained by HEG95 from integrated [OI] fluxes, the improved asymptotic value is a factor of 10 lower in DG Tau (Lavalley-Fouquet *et al.* 2000), similar in RW Aur (Woitas *et al.* 2002), and a factor 10 higher in RY Tau (Agra-Amboage *et al.*, submitted). Thus, HEG95 mass-loss rates currently do not appear to
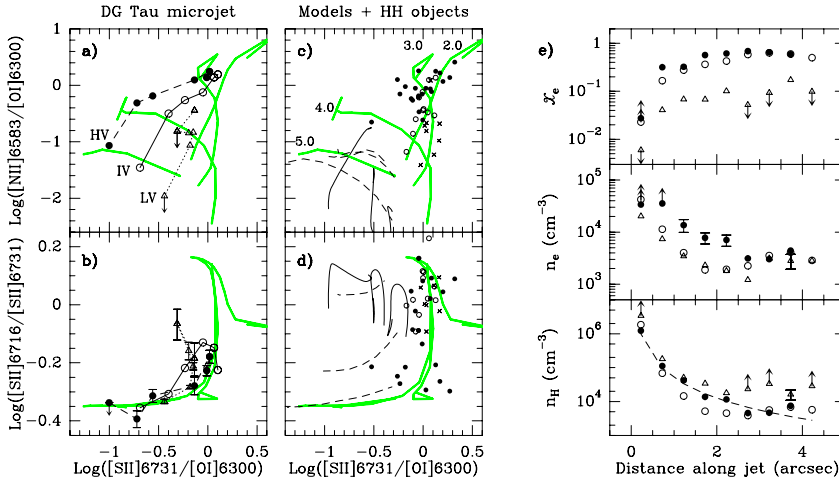
Figure 2. *Left:* Line ratios along the DG Tau microjet in 3 velocity intervals (large connected symbols in a,b) agree much better with predictions for planar shocks (thick green curves), than with ambipolar diffusion heating (thin solid in c,d) or viscous mixing-layers (dashed in c,d). The same is true for HH objects (small symbols in c,d). *Right:* Ionisation fraction x_e, electronic density n_e, and total density $n_H = n_e/x_e$ along the DG Tau jet, inferred from line ratios with the BE99 technique (Bacciotti & Eislöffel 1999). All panels from Lavalley-Fouquet *et al.* (2000). See also Dougados *et al.* (2002) for a similar analysis in the RW Aur microjet.

suffer from a large systematic bias and should remain useful for a statistical analysis. Combining them with updated $\dot{M}_{acc}$ values from Muzerolle *et al.* (1998), and adding the 3 revised $\dot{M}_j$ from spectroimaging, one obtains $\dot{M}_j/\dot{M}_{acc} \simeq 0.05$–$0.1$ (filled symbols in Figure 1). The same is found for 3 resolved Class I jets assuming $L_{bol} = L_{acc}$ (Hartigan *et al.* 1994; Cabrit 2002). Multiplying by 2 to account for the occulted redshifted jet yields $f \equiv (2\dot{M}_j)/\dot{M}_{acc} \simeq 0.1 - 0.2$, and $2L_j \simeq 0.1L_{acc}$ within a factor 2–3.

3. The need for MHD self-collimation of jets in CTTS

External collimation of an isotropic wind is difficult to reconcile with current constraints on the jet collimation scale (Cabrit 2007). The main arguments are summarized below, for a typical mass-loss rate of $\dot{M}_w = 10^{-8}$ $M_\odot\mathrm{yr}^{-1}$ and $\dot{M}_{acc} = 10^{-7}$ $M_\odot\mathrm{yr}^{-1}$.

3.1. External hydrodynamical collimation

An isotropic hydrodynamical wind is refocussed into a polar jet at distance Z_{max} if the ambient pressure P_0 is comparable to the wind ram pressure there: $P_0 \simeq \dot{M}_w V_w/(4\pi Z_{max}^2)$ (Barral & Cantó 1981; Cabrit 2007). With $V_w = 300\mathrm{km\ s}^{-1}$, $Z_{max} = 50$ AU, and the additional constraint that $n_{coll} \leqslant 4 \times 10^6$ cm^{-3} over this scale ($A_V \leqslant 3$mag in T Tauri stars), one would need hot material at $T > 6000$ K, only expected in a photoionised flow from the disk surface. Such a thermal flow reaches a speed $v_{evap} \simeq 30$ km s^{-1} (Font *et al.* 2004), ie 1/10th that of the wind. Thus, even including its ram pressure, it would need a mass-flux of $10 \times \dot{M}_w = 10^{-7}$ $M_\odot\mathrm{yr}^{-1}$ to refocus it. This is 1000 times more than the typical disk evaporation rate for a CTTS (Font *et al.* 2004) and comparable to the disk accretion rate, which is excluded.

Collimation by external hydrodynamic pressure may thus be safely ruled out. This conclusion is reinforced by the identical width of the molecular microjet of the HH212
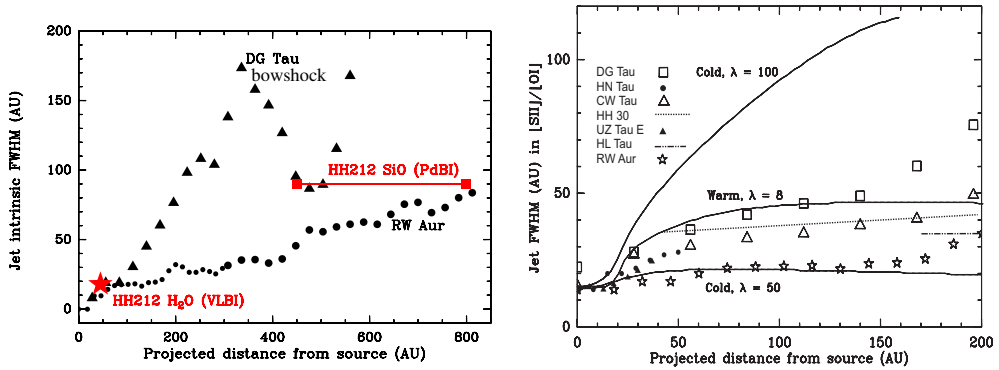
Figure 3. *Left:* Deconvolved width of the molecular microjet in HH212 (in red) compared with the full range encountered in atomic T Tauri jets. From Cabrit *et al.* (2007). *Right:* Predicted beam-convolved jet widths for self-similar cold and warm MHD disk winds at $z \leqslant 200$ AU (solid curves), compared with CTTS microjets (symbols). From Ray *et al.* (2007) and refs. therein

Class 0 source vs. atomic T Tauri jets, demonstrating that a dense infalling Class 0 envelope does not affect jet collimation (Cabrit *et al.* 2007, see left panel of Fig 3).

3.2. *External magnetic collimation*

Replacing P_0 above by $B_{\rm coll}^2/8\pi$ and keeping the same wind parameters one obtains a rough indication of the poloidal field that would focus an isotropic CTTS wind into a jet at z=50 AU: $B_{\rm coll} \simeq 10$ mG. For jet collimation to be effective, the field should be anchored over a disk region of radius $r_D \simeq 100$ AU $\gg r_j$ (Kwan & Tademaru 1988). The corresponding trapped flux would be $(\Phi_B)_{\rm coll} = \pi r_D^2 B_{\rm coll} = 8 \times 10^{28}$G cm^2, i.e., *at least* 2% of the flux present before gravitational collapse $(\Phi_B)_{\rm init} < (\Phi_B)_{\rm crit} = M\sqrt{G}/0.13 = 4 \times 10^{30}(M/1M_\odot)$G cm^2 (Mouschovias & Spitzer 1976). In contrast, 3D numerical MHD simulations of collapse find that only 0.1% of the initial flux remains in the disk, due to ohmic field diffusion (see contribution by Inutsuka, this volume).

Shu *et al.* (2007, and this volume) investigate an alternative scenario where 25% of the critical flux is conserved within 100 AU. External collimation could then occur on observed scales. However, the strong field also causes subkeplerian disk rotation, by 65% in CTTS. The predicted systematic discrepancy of a factor 1/0.4 between theoretical tracks and dynamical masses from disk rotation curves in CO does not appear supported by observations (White *et al.* 1999, Simon *et al.* 2000).

Finally, "active" external magnetic confinement may be provided by a self-collimated outer magnetized disk wind, but the latter would dominate the overall jet mass-flux (Meliani *et al.* 2006). A *purely passive, external* magnetic collimation of T Tauri jets therefore also appears unlikely.

3.3. *MHD self-collimation*

Any MHD wind launched along rotating open field lines tends to undergo self-collimation towards the spin axis (Bogovalov & Tsinganos 1999 and refs. therein). Collimation is achieved by the *toroidal* field component created by the wind inertia and not by the poloidal component. Therefore, it is much more efficient than external magnetic collimation in terms of required flux. For example, in self-similar MHD disk winds, the magnetic flux within the jet launch region $r_{out} \leqslant 1$–10 AU is $\Phi_B \leqslant 10^{26} - 10^{27}$ G cm^2 for $\dot{M}_{\rm acc}$= $10^{-7} M_\odot {\rm yr}^{-1}$ (cf. Eq. (19) in Ferreira *et al.* 2006), ie 2–3 orders of magnitude smaller than for external magnetic collimation, and less than 0.1% of the primordial flux.
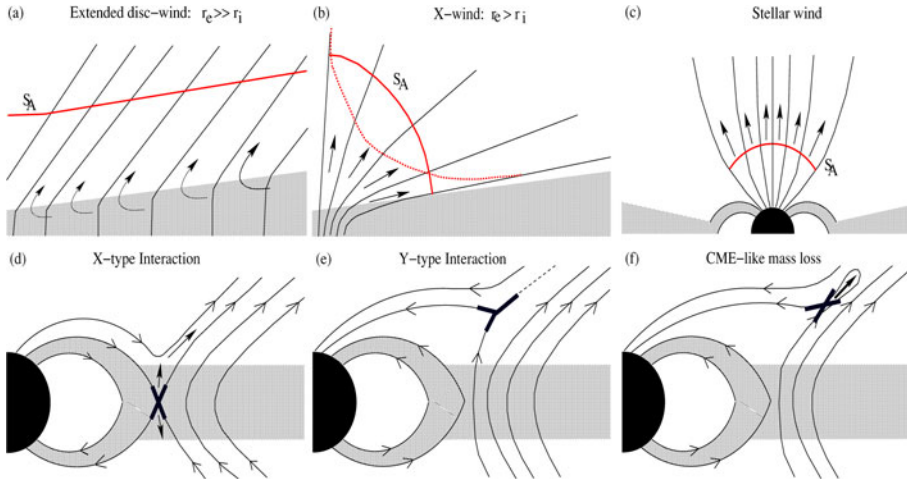
Figure 4. Possible launchsites for MHD winds in young accreting stars. Only those in Panels a) to d) are self-collimated. See Ferreira *et al.* (2006) for details.

Given the large flux loss expected during collapse, it thus seems most probable that CTTS jets trace *self-collimated MHD wind(s)*. Ferreira *et al.* (2006) distinguish four possible launch sites for such winds, illustrated in Fig. 4: (a) extended disk winds, (b) inner disk winds ("X-winds"), (c) stellar winds, (d) reconnexion X-winds ("ReX-winds"). In the following, we confront each of the four options against large-scale jet properties.

4. Pressure-driven MHD stellar winds

Helium line profiles indicate that stellar winds are present in at least 60% of CTTS (see Edwards, this volume; Kwan *et al.* 2007). If they were the main agent regulating angular momentum in CTTS, their mass-loss rate would be $\simeq 0.1$ of $\dot{M}_{\rm acc}$ (Matt & Pudritz 2005). Therefore they are a prime candidate for the origin of T Tauri jets.

4.1. *Jet collimation*

Current analytical and numerical models of MHD stellar winds predict a narrow region of cylindrical flow with radius $\leqslant$ 10–20 Alfvén radii, i.e., $\leqslant 200R_\star \simeq 2$ AU (eg. Sauty & Tsinganos 1994; Bogovalov & Tsinganos 2001). Possible ways to reproduce the apparent jet radii of 10–20 AU, eg. through density collimation or enhanced mass-flux at intermediate latitudes, remain to be investigated.

4.2. *Jet poloidal speeds along and transverse to the axis*

CTTS stellar winds probed in Helium lines reach a speed similar to that of the large-scale jets (Edwards *et al.* 2003). Since T Tauri stars rotate at only 10% of break-up, centrifugal launching is ineffective and strong pressure gradients are needed to accelerate the gas. Following Ferreira *et al.* (2006), the asymptotic speed may be written $V_j = \sqrt{(\beta-2)GM_\star/R_\star}$ where $\beta = 2(\Delta H + \mathcal{F})/(GM_\star/R_\star)$ parametrises the amount of energy given to the flow from enthalpy gradients, Alfvén wave pressure, etc.

Observed HVC speeds of $1-2$ times the stellar keplerian speed thus require $\beta \simeq 3-6$. This is only slightly changed by the effect of centrifugal acceleration, as the star rotates slowly (cf. Fig. 7 and Ferreira *et al.* 2006). The strong transverse velocity decrease observed in several jets could be reproduced, eg. if β drops at lower latitudes, or if the last stellar field line is recollimated by a disk field, allowing the development of slower bowshocks/turbulent wakes around the fast jet beam.

4.3. *Constraints on jet rotation*

Magnetised stellar winds carry a specific angular momentum of

$$\lambda_\star \Omega_\star R_\star^2 = 70 \left(\frac{\delta}{0.1}\right) \left(\frac{\lambda_\star}{200}\right) \left(\frac{M_\star}{M_\odot}\right)^{1/2} \left(\frac{R_\star}{3R_\odot}\right)^{1/2} \text{AU km s}^{-1}, \qquad (4.1)$$

where $\delta \simeq 0.1$ is the fraction of break-up speed at which the star rotates. The predicted locus is shown in blue in Fig. 7. It does not reproduce the large values of 200–300 AU km s^{-1} reported towards jet edges. However, detected velocity shifts $\leqslant 20$ km s^{-1} might also arise from other effects than rotation, eg. an asymmetric interaction with the ambient medium or a slight jet precession (Soker 2005; Cerqueira *et al.* 2006). RW Aur, where the gradient is clearly inconsistent with the disk rotation sense, and HH212, where the transverse shifts are opposite in H_2 and SiO knots, are two cases in point (Cabrit *et al.* 2006; Codella *et al.* 2007). Until the data are more discriminant, they are not a decisive argument to exclude stellar winds as the origin of CTTS jets.

4.4. *Jet ejection to accretion ratio*

The large optical depth and unknown geometry of CTTS stellar winds currently prevent an accurate measure of their contribution to the jet mass-flux. But the following theoretical arguments, from Ferreira et al. (2006), show that an ejection/accretion ratio $\simeq 0.2$ would be challenging: with $\beta \simeq 3$, the net energy input in the two jets would be:

$$L_\beta = \frac{\beta}{2} \frac{GM_\star}{R_\star} (2\dot{M}_j) = \beta \left(\frac{\dot{M}_j}{\dot{M}_a}\right) L_{\text{acc}} \simeq 30\% L_{\text{acc}}. \qquad (4.2)$$

If energy were provided in the form of enthalpy, the true total heating rate *including radiative losses* would then be excessive (cf. Matt, this volume; De Campli 1981). In addition, CTTS stellar winds appear cooler than 20,000 K in their acceleration region (Johns-Krull & Herczeg 2007), also arguing against significant enthalpy gradients.

Non-thermal acceleration by Alfvén wave pressure gradients meets a similar efficiency problem. For $B_\star = 150\text{-}500$ G and a final speed of 300 km s^{-1}, De Campli (1981) found that the required power in *coherent* Alfvén waves is $5 - 10$ times the jet power, i.e., 50%-100% of L$_{\text{acc}}$. This sounds prohibitive, as incoherent Alfvén waves and dissipative waves (acoustic, magnetosonic) will be excited as well. Note that De Campli concluded otherwise because he was comparing the wave power to the total stellar luminosity, not to L$_{\text{acc}}$ which is typically much smaller in CTTS.

A more promising pressure-drive for stellar winds is the "magnetic coil" push produced by strongly twisted open field lines in the stellar corona. This effect is observed in numerical simulations (see contributions by Inutsuka and by Romanova, this volume) but may be transient. Unless it proves to be long-lived and efficient enough, pressure-driven stellar winds would provide no more than $\simeq 10\%$ of the mass-flux in T Tauri jets.

5. Inner disk winds: The "X-wind" model(s)

In the X-wind scenario, a steady-state "disk-locking" is assumed, where angular momentum accreted through funnel flows is balanced by angular momentum deposited slightly outside corotation by trailing closed stellar field lines. The excess angular momentum deposited in the disk is then assumed to power a centrifugal outflow from a tiny region beyond this point, along field lines that have been disconnected from the star. Using a prescribed mass-loading function, the Alfvén surface and asymptotic collimation
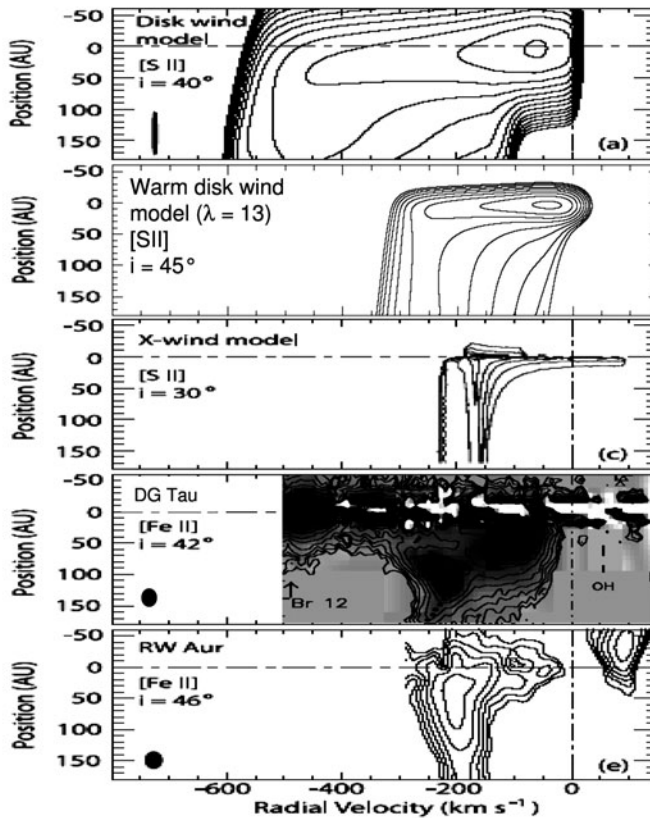
Figure 5. Observed and synthetic PV diagrams of T Tauri microjets along the jet axis (adapted from Pyo *et al.* 2006): the warm disk wind model in (b) is from Cabrit *et al.* (in prep), and the DG Tau PV diagram in (d) is from Pyo *et al.* (2003).

were calculated in the case of no external disk field, making several specific predictions that can be compared with observations (Najita & Shu 1994; Shu *et al.* 1995).

5.1. *Jet collimation*

Despite the presence of unrecollimated radial streamlines at wide angle, the X-wind quickly achieves a cylindrical *density* distribution. The jet beam is then somewhat of an "optical illusion" (Shang *et al.* 1998). Unconvolved synthetic maps yield a power-law transverse intensity distribution with a narrow core of 2 AU. PSF convolution would thus be needed for a definite comparison with observed jet widths.

5.2. *Jet poloidal speeds along and transverse to the axis*

The X-wind predicts a mean magnetic lever arm parameter $\bar{\lambda} = (r_A/r_o)^2 \simeq 3.5$ over most of the flow. Panel (c) of Fig. 5 shows an unconvolved synthetic PV cut along the jet calculated for a corotation radius $R_{\rm cor} = 12R_\odot$ and $V_{K,{\rm cor}} = 92$ km s^{-1} (Shang *et al.* 1998) corresponding to M$_\star = 0.5M_\odot$ and $P_\star = 6.6$ days, ie. typical of a CTTS like DG Tau. The mean (deprojected) terminal jet speed is then $\simeq 180$ km s^{-1}, with 10% of the mass flux reaching 270 km s^{-1}.
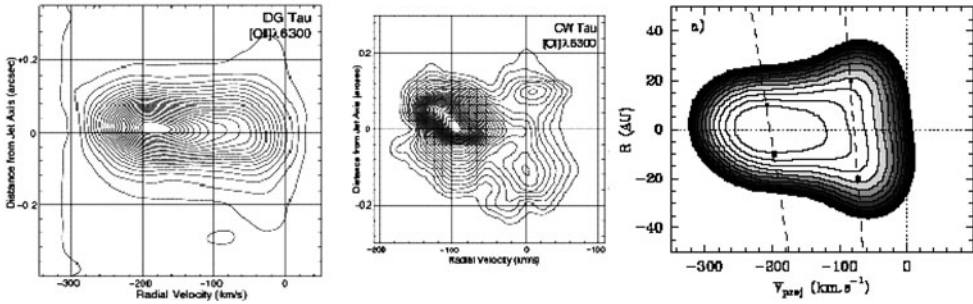
Figure 6. *Left and Middle:* Transverse PV diagrams at $z = 50$AU from HST illustrating the slower sheath at R = 15–30 AU around the fast jet core in DG Tau and CW Tau (adapted from Coffey *et al.* 2007). *Right:* Synthetic transverse PV diagram for the warm disk wind model fitting both the HVC and rotation data in the DG Tau jet, convolved at the HST/STIS resolution (from Peseneti *et al.* 2004).

The overall acceleration scale and the narrow HVC of RW Aur are both very well reproduced. On the other hand, the predicted HVC is a factor 2 too slow in DG Tau, and the bright IVC at velocities down to -50 km s^{-1} is not reproduced at all.

The wide-angle nature of the X-wind actually makes it very difficult to produce an IVC feature: the X-wind always contains unrecollimated *and* fast radial streamlines, with a ram pressure exceeding the circumstellar pressure of a CTTS by a factor $\simeq 1000$ at 50 AU (see § 3.1); thus, any layer of interaction with ambient gas will be pushed out to 1000 AU or beyond. In contrast, the slower "sheath" emitting the IVC lies at only 15–30 AU of the jet axis at $z = 50$ AU (see Fig. 6).

To develop such a narrow slow sheath, the last streamline of the X-wind should recollimate much faster. Such a modified geometry was mentioned by F. Shu at this conference, but the proposed confining disk field predicts subkeplerian disk rotation that does not seem supported by observations (cf. § 3.2). Jets with an IVC thus remain a challenge for X-wind model(s) as currently envisioned.

5.3. *Jet rotation*

The specific angular momentum carried away by the X-wind is

$$\lambda\Omega_\star R_{\rm cor}^2 = \lambda\Omega_{K,\star}R_\star^2\delta^{-1/3} = 22{-}44\left(\frac{\delta}{0.1}\right)^{-1/3}\left(\frac{M_\star}{M_\odot}\right)^{1/2}\left(\frac{R_\star}{3R_\odot}\right)^{1/2} {\rm AU\,km\,s}^{-1}. \quad (5.1)$$

The predicted locus in the $rV_\phi - V_p$ plane is indicated in Fig. 7. It falls near stellar winds with $\beta = 2$, $\lambda_\star = 50 - 150$, and is again compatible with current data if considered as upper limits to the true jet rotation.

5.4. *Ejection to accretion ratio*

Current predictions for the X-wind were calculated with a prescribed ejection/accretion ratio $f = 2\dot{M}_j/\dot{M}_{acc} \simeq 0.25$, compatible with the mean value in CTTS jets. The fact that $f\bar{\lambda} \simeq 1$ means that the total angular momentum flux carried away by the X-wind is equal to that extracted from the funnel flow by disk-locking: $\dot{M}_{\rm acc}\Omega_\star R_{\rm cor}^2$ (assuming a truncation radius close to corotation). However, the turbulent viscosity and steady-state disk structure required to transport the extracted angular momentum to the X-wind launch region, and to sustain the high mass-loading, have not yet been calculated.

6. Extended MHD disk winds

Magneto-centrifugal ejection from keplerian accretion disks is a well-understood jet formation process (see Fendt, this volume; Pudritz *et al.* 2007 and refs. therein). Steady, self-similar solutions including full treatment of the mass-loading have been calculated for vertically isothermal disks ("cold" disk winds, Ferreira 1997), and for disks with moderate surface heating ("warm" disk winds, Casse & Ferreira 2000). From these, a complete set of synthetic predictions was produced and tested against observational constraints, with the following results:

6.1. *Jet collimation*

As shown in the right panel of Fig. 3, beam-convolved synthetic maps for self-similar disk winds reproduce very well the observed jet FWHM as a function of distance, for an inner launch radius close to corotation ($r_{in} \simeq 0.07$ AU) and a magnetic lever arm parameter $\lambda < 70$ (Cabrit *et al.* 1999; Garcia *et al.* 2001). The outer launch radius has a minor effect, unless ionisation is much higher there than on-axis (Cabrit *et al.* 1999).

6.2. *Jet kinematics*

Disk winds are mainly magneto-centrifugally accelerated, with a negligible effect from enthalpy even in "warm" solutions ($\beta \ll 1$). The asymptotic speed along a stream-line with footpoint radius r_o and magnetic lever arm parameter $\lambda \simeq (r_A/r_o)^2$ is then $V_p^\infty(r_o) = \sqrt{GM_\star/r_o}\sqrt{2\lambda - 3}$ (cf. Blandford & Payne 1982). Convolved synthetic PV diagrams along the jet axis are presented in Fig. 5 for an inner launch radius $r_{in} = 0.07$ AU and an outer radius of 1–3 AU. The cold model in Fig. 5a has a large $\lambda \simeq 50$ that is seen to produce excessive jet speeds (cf. Garcia *et al.* 2001; Pyo *et al.* 2006). However, warm disk wind models can reach lower λ and adequate velocities (Casse & Ferreira 2000; Pesenti *et al.* 2004). The warm model with $\lambda = 13$ in Fig. 5b is now in excellent agreement with the HVC in the DG Tau PV diagram. The slower HVC in RW Aur could be reproduced with an even lower $\lambda \simeq 4 - 6$.

The warm model in Fig. 5b is also seen to naturally produce an IVC similar to that of DG Tau, as matter launched from large disk radii of 1– 3 AU achieves lower speeds (in proportion to the kepler speed at the anchoring radius). The transverse PV diagram for the same model is shown in Fig. 6, and fits well the observed transverse velocity decrease in DG Tau (as well as the associated rotation signatures, see Pesenti *et al.* 2004 and below). On the other hand, jets without an IVC, such as in RW Aur, are not as easily explained as they need ad-hoc assumptions (Cabrit *et al.* in prep).

6.3. *Jet rotation*

As illustrated in Fig. 7, the combination of rotation and poloidal speed in an MHD wind from a keplerian disk allows to derive both the launch radius (Anderson *et al.* 2003) and a lower limit λ_ϕ to the wind lever arm parameter λ (Ferreira *et al.* 2006). Current rotation estimates in the IVC of two jets, DG Tau and Th28-Red, would indicate launch radii r_{out} of 1 AU to 3 AU for the slow sheath (cf. Bacciotti *et al.* 2002; Coffey *et al.* 2004; Fendt 2006), and a true magnetic lever arm parameter $\lambda \simeq 13$ (Pesenti *et al.* 2004). This is the same range of λ as inferred independently from HVC maximum speeds (see above). Thus, the HVC and IVC components could be interpreted as inner and outer streamlines of the same extended MHD disk wind, if the rotation interpretation is confirmed.
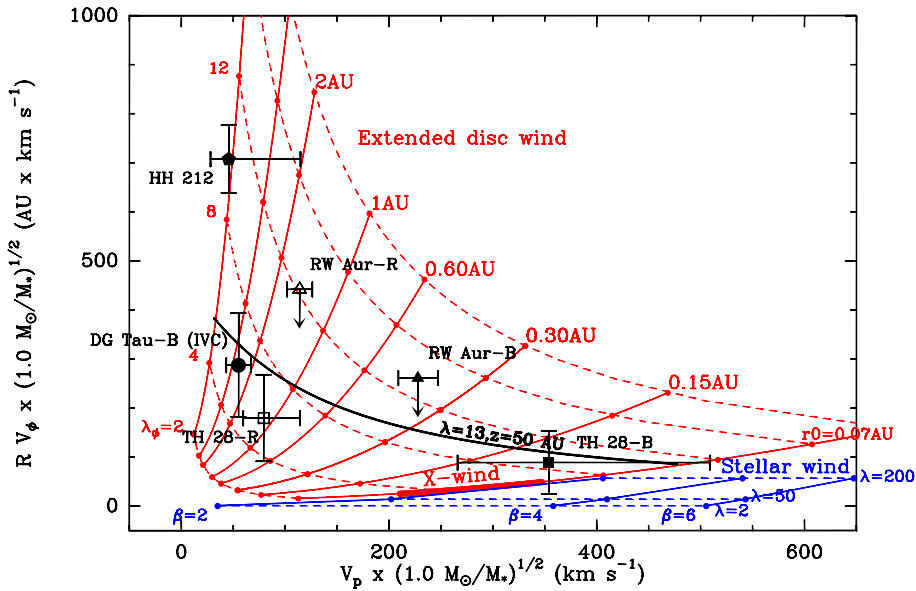
Figure 7. Constraints in the $V_p - rV_\phi$ plane on the launch point r_o and effective magnetic lever arm λ_ϕ of steady extended MHD disk winds. The thick black curve shows a cut at $z = 50$ AU across a warm disk wind solution with $\lambda = 13$. The locus of the X-wind and stellar winds with various pressure parameters β is also indicated. Symbols show current measurements; they are only upper limits for RW Aur and HH212 (see §4.3). From Ferreira *et al.* (2006).

6.4. *Ejection to accretion ratio*

The mass ejection to accretion ratio in a self-similar extended disk wind is given by

$$2\dot{M}_j/\dot{M}_{acc} \simeq \frac{\ln(r_{out}/r_{in})}{(2\lambda - 2)}. \tag{6.1}$$

With $\lambda \simeq 6 - 13$, and $r_{out}/r_{in} \simeq 10 - 40$ (from IVC rotation data), one could reach a total ejection/accretion ratio $\simeq 0.15 - 0.2$ compatible with the mean observed ratio in CTTS jets (Ferreira *et al.* 2006). Note however that an extended MHD disk wind brakes only the disk, not the star. If the stellar wind is not sufficient for this purpose, excess angular momentum accreted from the inner disk edge would have to be removed by another agent, possibly a reconnexion X-wind (see below).

7. The reconnection X-wind model ("ReX-wind")

When the stellar and disk magnetic moments are parallel — instead of anti-parallel as assumed in the X-wind model — a magnetic X-point forms at the magnetopause. This leads to a fourth type of self-collimated MHD ejection illustrated in panel (d) of Fig. 4, triggered by reconnexion between closed stellar loops and open disk field.

As shown by Ferreira *et al.* (2000; see also Ferreira, this volume), this centrifugal "reconnexion X-wind" (hereafter ReX-wind) flows along newly opened field lines anchored *in the star*, not in the disk. It thus brakes down the star very efficiently, without the need for previous angular momentum extraction through disk-locking as in the X-wind scenario. Assuming a magnetopause close to corotation, the condition to maintain a slow rotation in CTTS despite accretion would again write $f\lambda \simeq 1$. Since matter is lifted up above the magnetic X-point by magnetic pressure, not just by the disk hydrostatic

pressure gradient, one might expect a high mass-loading efficiency $f \simeq 0.1 - 0.3$. With $\lambda = 1/f \simeq 3 - 10$, the ReX wind would then reproduce both the HVC mass and speed.

In contrast to the X-wind, the ReX wind would not fan out over a wide-angle but would be automatically confined by the outer poloidal disk field that feeds reconnexion. The observed sheath of intermediate/low velocity material, currently unexplained in X-wind scenarii (see §5), could naturally develop at this interface and/or through an extended MHD disk wind launched further out.

8. Conclusions

The collimation of jets in CTTS cannot be due to external hydrodynamical pressure and most likely results from MHD self-collimation along rotating open field lines. CTTS jets are thus an important agent of angular momentum removal from the star or disk. A detailed comparison of theoretical model predictions with spatially resolved jets properties reveals open issues with most scenarii for the jet origin:

- Stellar winds are present in CTTS and reach adequate terminal speeds but they do not seem able to provide more than 10% of the jet mass-flux, unless efficient acceleration by a "magnetic coil" is operative. Further research along this line is definitely needed, including insight from both numerical and laboratory experiments (eg. the "magnetic tower" jets studied by Lebedev *et al.* 2005).

- The X-wind is successful in producing a narrow HVC. However, its wide-angle nature prevents the formation of a sheath of lower velocity gas at 15–30 AU of the jet axis. A much tighter recollimation of outer streamlines would be required, with a disk field compatible with the observed keplerian disk rotation.

- Conversely, extended "warm" MHD disk winds agree very well with observational constraints in jets with a low-velocity sheath (Ferreira *et al.* 2006), but they may have difficulties reproducing the properties of jets with an HVC only (Cabrit *et al.* in prep.).

- Reconnexion X-winds are very promising as they seem potentially able at the same time to brake down the star, produce an HVC with sufficient mass and speed, and develop a lower velocity sheath around the jet beam. Modelling of the wind dynamics and geometry would be essential for a closer comparison with observations.

References

Anderson, J.M., Li, Z.-Y., Krasnopolsky, R., & Blandford, R. 2003, ApJ 590, L107
Bacciotti, F., & Eislöffel, J. 1999, A&A 342, 717 (BE99)
Bacciotti, F., Mundt, R., Ray, T.P., Eislöffel, J., Solf, J., & Camenzind, M. 2000, ApJ 537, L49
Bacciotti, F., Ray, T. P., Mundt, R., Eislöffel, J., & Solf, J. 2002, ApJ 576, 222
Barral, J. F., & Canto, J. 1981, RMxAA 5, 101
Blandford, R.D., & Payne D.G. 1982, MNRAS 199, 883
Bogovalov, S., & Tsinganos, K.1999, MNRAS 305, 211
Bogovalov, S., & Tsinganos, K. 2001, MNRAS 325, 249
Cabrit, S. 2002, in: *Star Formation and the Physics of Young Stars*, ed. by J. Bouvier, J.-P. Zahn (EDP Sciences, Les Ulis 2002) pp. 147–182
Cabrit 2007, in *MHD jets and winds from young stars*, eds. J. Ferreira, C. Dougados et E. Whelan, Lecture Notes in Physics (Spinger), in press.
Cabrit, S., Edwards, S., Strom, S.E., & Strom, K.M. 1990, ApJ 354, 687

Cabrit, S., Ferreira, J., & Raga, A.C. 1999, A&A 343, L61

Cabrit, S., Pety, J., Pesenti, N., & Dougados, C. 2006, A&A, 452, 897

Cabrit, S., *et al.* 2007, A&A 468, L29

Casse, F., & Ferreira, J. 2000, A&A 361, 1178

Cerqueira, A. H., Velázquez, P. F., Raga, A. C., Vasconcelos, M. J., & de Colle, F. 2006, A&A 448, 231

Codella, C. *et al.* 2007, A&A 462, L53

Coffey, D., Bacciotti, F., Woitas, J., Ray, T. P., & Eislöffel, J. 2004, ApJ 604, 758

Coffey, D., Bacciotti, F., Ray, T. P., Eislöffel, J., & Woitas, J. 2007, ApJ 663, 350

De Campli, W.M. 1981, ApJ 244, 124

Dougados, C., Cabrit, S., Lavalley-Fouquet, C., & Ménard, F. 2000, A&A 357, L61

Dougados, C., Cabrit, S., Lavalley-Fouquet, C. 2002, RMxAA Conf. Ser. 13, 43

Edwards, S., *et al.* 2003, ApJ 599, L41

Fendt, C. 2006, ApJ 651, 272

Ferreira, J. 1997, A&A 319, 340

Ferreira, J., & Pelletier, G., Appl, S. 2000, MNRAS 312, 387

Ferreira, J., Dougados, C., & Cabrit, S. 2006, A&A 453, 785

Font, A., McCarthy, I.G., Johnstone, D., & Ballantyne, D.R. 2004, ApJ 607, 890

Garcia, P., Cabrit, S., Ferreira, J., & Binette, L. 2001, A&A 377, 609

Hartigan, P., Morse, J., & Raymond,. J. 1994, ApJ 436, 125

Hartigan, P., Edwards, S., & Gandhour, L. 1995, ApJ 452, 736 (HEG95)

Hartigan, P., Edwards, S., Pierson, R. 2004, ApJ 609, 261

Johns-Krull, C. M., & Herczeg, G. J. 2007, ApJ 655, 345

Kwan, J., Tademaru, E. 1988, ApJ 332, L41

Kwan, J., Edwards, S., & Fischer, W. 2007, ApJ 657, 897

Lavalley-Fouquet, C., Cabrit, S., & Dougados, C. 2000, A&A 356, L41

Lebedev, S.V., *et al.* 2005, MNRAS 361, 97

Matt, S., & Pudritz, R. 2005, ApJ 632, L135

Meliani, Z., Casse, F., & Sauty, C. 2006, A&A 460, 1

Mouschovias, T., & Spitzer, L. 1976, ApJ 210, 326

Muzerolle, J., Hartmann, L., & Calvet, N. 1998, AJ 116, 2965

Najita, J.R., & Shu, F.H. 1994, ApJ 429, 808

Pesenti, N., *et al.* 2004, A&A 416, L9

Pudritz, R.E., Ouyed, R., Fendt, C. & Brandenburg, A. 2007. In *Protostars & Planets V*, ed. by B. Reipurth, D. Jewitt, K. Keil, (University of Arizona Press, Tucson), in press

Pyo, T.-S. *et al.* 2003, ApJ 590, 340

Pyo, T.-S. *et al.* 2006, ApJ 649, 836

Ray, T.P., Mundt, R., Dyson, J.E., Falle, S.A.E., Raga, A. 1996, ApJ 468, L103

Ray, T.P. *et al.* 2007, In *Protostars & Planets V*, ed. by B. Reipurth, D. Jewitt, K. Keil, (University of Arizona Press, Tucson), in press.

Sauty, C., & Tsinganos, K. 1994, A&A 287, 893

Shang, H., Shu, F.H., & Glassgold, A.E. 1998, ApJ 493, L91

Shu, F.H., Najita, J., Ostriker, E.C., & Shang, H. 1995, ApJ 455, L155

Shu, F.H., Galli, D., Lizano, S., Glassgold, A.E., & Diamond, P. 2007, submitted

Simon, M., Dutrey, A., & Guilloteau, S. 2000, ApJ 545, 1034

Soker, N. 2005, A&A 435, 125

Stapelfeldt, K. *et al.* 2003, ApJ 589, 410

White, R. J., Ghez, A. M., Reid, I. N., & Schultz, G. 1999, ApJ 520, 811

Woitas, J., Ray, T.P., Bacciotti, F., Davis, C.J., & Eislöffel, J. 2002, ApJ 580, 336